miR-21-5p targets *SKP2* to reduce osteoclastogenesis in a mouse model of osteoporosis

Yizhen Huang[1,2,‡], Yute Yang[1,2,‡], Jianle Wang[1,2,‡], Shasha Yao[1,2], Teng Yao[1,2], Yining Xu[3], Zizheng Chen[1,2], Putao Yuan[1,2], Jun Gao[1,2], Shuying Shen[1,2,*], and Jianjun Ma[1,2,*]

From the [1]Department of Orthopaedic Surgery, Sir Run Run Shaw Hospital, Zhejiang University School of Medicine, Hangzhou, China; [2]Key Laboratory of Musculoskeletal System Degeneration and Regeneration Translational Research of Zhejiang Province, Hangzhou, China; and [3]School of Medicine, Shaoxing University, Shaoxing, China

Edited by Karin Musier-Forsyth

Osteoporosis results from an imbalance between bone formation and bone resorption. Traditional drugs for treating osteoporosis are associated with serious side effects, and thus, new treatment methods are required. This study investigated the role of differentially expressed microRNAs during osteoclast differentiation and osteoclast activity during osteoarthritis as well as the associated underlying mechanisms. We used a microarray to screen microRNAs that decreased in the process of osteoclast differentiation and verified miR-21-5p to decrease significantly using RT-qPCR. In follow-up experiments, we found that miR-21-5p targets *SKP2* to regulate osteoclast differentiation. *In vivo*, ovariectomized mice were used to simulate perimenopausal osteoporosis induced by estrogen deficiency, and miR-21-5p treatment inhibited bone resorption and maintained bone cortex and trabecular structure. These results suggest that miR-21-5p is a new therapeutic target for osteoporosis.

Bone resorption of osteoclasts and formation of osteoblasts maintain homeostasis of bone tissue (1). Osteoporosis occurs when bone resorption is greater than formation (2), and although it develops in both sexes, it is more prevalent in postmenopausal females and elderly males (3). The primarily available treatment against osteoporosis includes calcium, calcitonin, diphosphate, and estrogen. Calcium supplementation prevents and treats osteoporosis; however, its long-term use can induce nausea, vomiting, and indigestion. Moreover, since the absorption capacity declines with age, calcium efficacy in preventing and treating osteoporosis in elderly individuals is limited (4). Calcitonin is effective in preventing and healing of new pyramidal fractures but also associated with side effects including nausea, vomiting, and flushing, and hence it is commonly used as a second-line therapy to treat osteoporosis (5). Bisphosphonates induce apoptosis in osteoclasts, thereby decreasing bone transformation, making them an ideal treatment option; however, long-term use can lead to overinhibition of bone remodeling and repair, resulting in excessive bone mineralization and destruction of bone microstructure (6). Estrogen is the most effective treatment strategy for postmenopausal females with osteoporosis; however, hormone replacement therapy is associated with adverse reactions in other systems. Estrogen is contraindicated in patients with allergies, breast cancer, thrombophlebitis, and vaginal bleeding of an unclear diagnosis, and is not used for osteoporosis treatment (7). Considering all the above treatment options, safer and more effective treatments and prevention strategies for osteoporosis remain warranted.

microRNAs are short sequences RNA with a length of approximately 20 to 24 nt that do not encode proteins. Accumulating evidence has illustrated the important role of miRNAs in osteoporosis (8). In recent studies, it has been found that microRNA-29a reduces osteoclast differentiation by inhibiting osteoclast regulators RANKL and CXCL12 (9). In addition, the expression of microRNA-148a in osteoporosis rat model following ovariectomy has been shown to be significantly upregulated and that it can affect osteoporosis through ERα by the PI3K/AKT axis (10). The authors also investigated the role of microRNA-449b-5p in osteogenic differentiation of bone marrow mesenchymal stem cells (BMSCs) and found that microRNA-449b-5p could aggravate osteoporosis by inhibiting osteogenic differentiation through targeting Satb2 (11). Therefore, investigating miRNAs in osteoporosis may provide an insight into new therapeutic targets.

S-Phase Kinase-Associated Protein 2 (*SKP2*) is a protein-coding gene, which significantly affects cell cycle regulation (12). In breast cancer, *SKP2* promotes tumourigenesis and radiation tolerance by degrading PDCD4 (13). Runx2, an osteogenic transcription factor, affects osteoblasts differentiation; *SKP2* inhibits osteogenesis through ubiquitin-mediated degradation of Runx2 (14). In this study, we hypothesize that *SKP2* is a target gene of miR-21-5p and verified the function of *SKP2* in osteoclastic differentiation.

To better understand these effects, we screened miRNAs differentially expressed during receptor activator of nuclear factor kappa B ligand (RANKL)-induced osteoclast differentiation *in vitro* using RAW264.7 cells. Based on the screening results, we focused on miR-21-5p as a potential target for osteoporosis treatment, which was downregulated in mature osteoclasts.

‡ These authors contributed equally to this work.
* For correspondence: Shuying Shen, 11207057@zju.edu.cn; Jianjun Ma, sealteam@zju.edu.cn.

Bioinformatics analysis was conducted to predict target genes of miR-21-5p. Moreover, we evaluated the influence of a precursor miR-21-5p drug in the prevention of osteoporosis in ovariectomized (OVX) mice to determine the therapeutic potential.

Results

RANKL-induced RAW264.7 cells differentiation into osteoclasts

TRAP-positive multinucleated cells were observed in the RANKL-stimulated group, whereas no TRAP-positive cells were found in the control group (Fig. 1A). In addition, RT-qPCR analysis showed that the mRNA expression levels of *TRAP* and *cathepsin K* were increased in the RANKL-induced group compared with those in the control group (Fig. 1B) (15). Mouse bone marrow macrophages (BMMs) were induced by M-CSF and RANKL, and depressions in the surface of the bone slice were observed (Fig. 1C) (16). These results confirmed

RANKL induction of macrophages differentiation into osteoclasts. We selected five pairs of samples for sequencing, which were not induced by RANKL or RANKL, for 5 days. Twenty out of the microRNAs significantly downregulated ($p < 0.05$, logFC < -2) during osteoclastic differentiation were selected (Fig. 1D). Furthermore, we detected the expression of microRNAs ($p < 0.05$, logFC < -3) during osteoclast differentiation using RT-qPCR (Fig. 1E). Among them, the expression of miR-21-5p decreased most significantly, and hence was selected for further investigations, and speculated that it can inhibit osteoclast growth, differentiation, or function.

MiR-21-5p inhibited osteoclast differentiation

To further investigate the role of miR-21-5p in osteoclastogenesis as a potential target for osteoporosis treatment, RAW264.7 cells were transfected with vectors to silence or
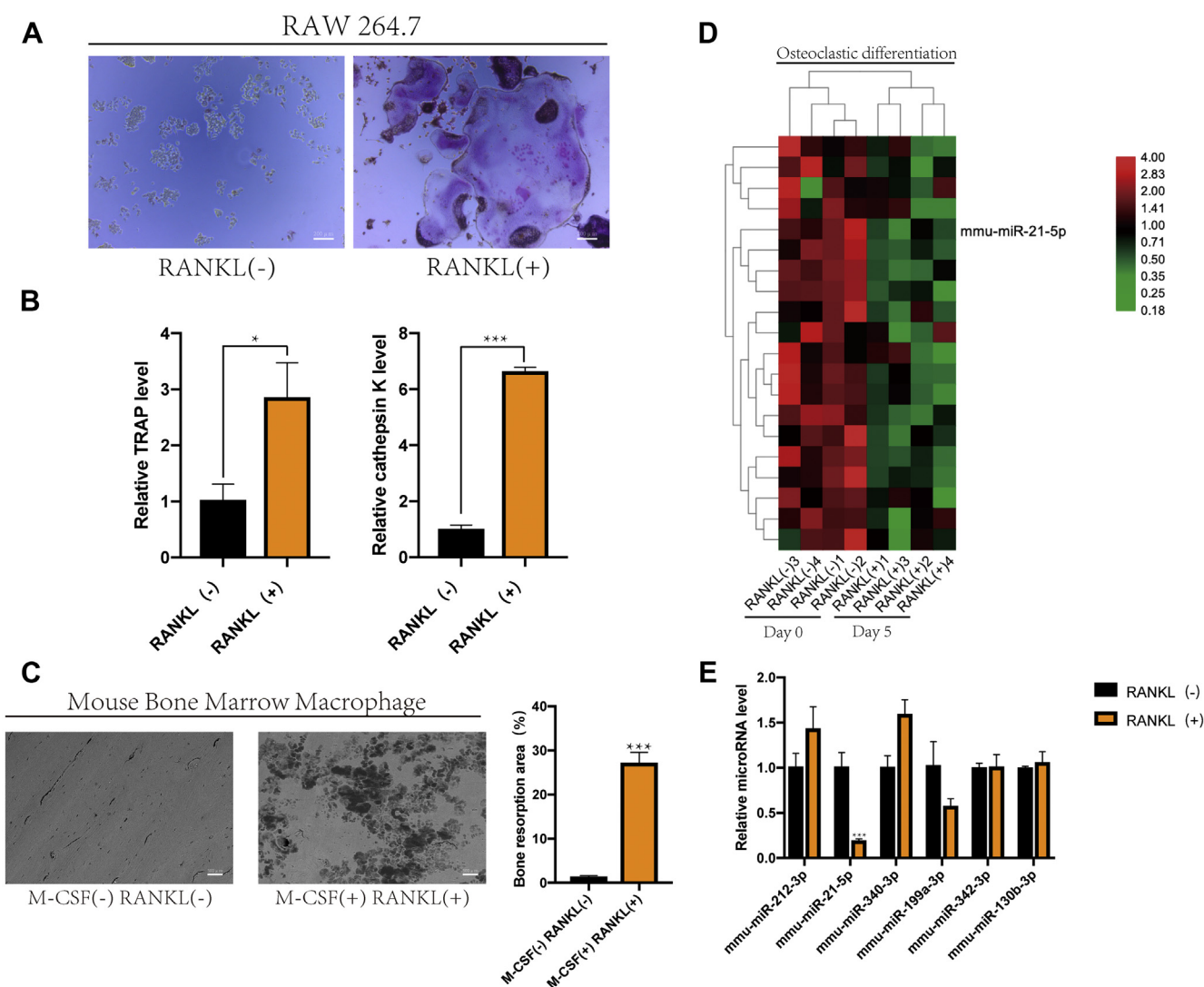
Figure 1. RAW264.7 cells were induced to differentiate into osteoclasts by RANKL. *A*, RAW264.7 cells were cultured in α-MEM containing RANKL (50 ng/ml) for 120 h, and TRAP staining was used to analyze osteoclast activity (scale bar, 200 μm). *B*, RAW264.7 cells were stimulated with RANKL (50 ng/ml) for 120 h. The relative mRNA expression levels of TRAP and cathepsin K were analyzed using RT-qPCR. *C*, bone resorption test showed different pit sizes, which represented the activity of osteoclasts (scale bar, 500 μm). The defect area was analyzed quantitatively. *D*, expression of miRNAs in RAW264.7 cells during osteoclast differentiation detected by microarray assays. *Red* and *green* represent high and low expression, respectively. *E*, the expression levels of microRNAs were determined using RT-qPCR. (*$p < 0.05$, **$p < 0.01$, ***$p < 0.001$. Data represent mean ± S.D. and the p values were determined by a two-tailed unpaired Student's *t*-test.)
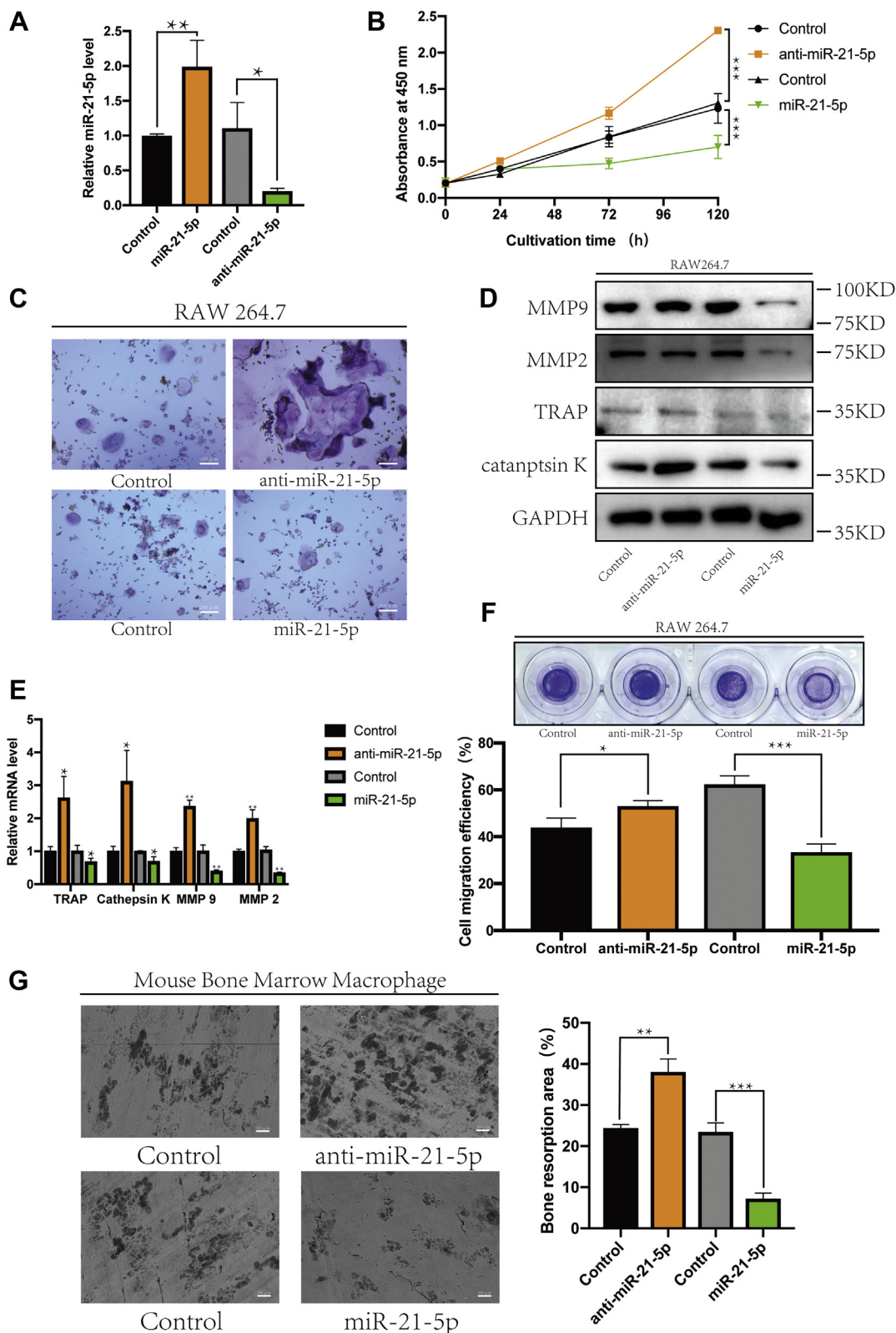
Figure 2. MiR-21-5p inhibited osteoclast differentiation. *A*, MiR-21-5p or anti-miR-21-5p was transfected into RAW264.7 cells, and the expression of miR-21-5p was detected using RT-qPCR. *B*, RAW264.7 cells were cultured in α-MEM containing RANKL (50 ng/ml) for 120 h. The effect on cell proliferation was detected using the CCK-8 assay. *C*, osteoclast activity was detected using TRAP staining (scale bar, 200 μm). The protein and transcript expression levels of TRAP, cathepsin K, MMP-9, and MMP-2 were determined using (*D*) western blot and (*E*) RT-qPCR. *Gapdh* was used as an internal reference gene. Migration was detected by (*F*) a Transwell assay, and migration efficiency was analyzed quantitatively. *G*, bone resorption test showed different size of pits, which represented the activity of osteoclasts (scale bar, 500 μm). The defect area was analyzed quantitatively. (*$p < 0.05$, **$p < 0.01$, ***$p < 0.001$. Data represent mean ± S.D. and the *p* values were determined using a two-tailed unpaired Student's *t*-test.)

overexpress miRNAs (Fig. 2A), followed by treatment with RANKL for osteoclast differentiation. CCK-8 assay showed that cell growth in the miR-21-5p overexpression group was weaker than that in the miR-21-5p-silenced group (Fig. 2B) (17). Similarly, TRAP staining of the induced osteoclasts showed numerous TRAP-positive multinucleated cells in the anti-miR-21-5p group, whereas osteoclast formation was inhibited in the miR-21-5p overexpression group (Fig. 2C) (18). Western blot and RT-qPCR further showed that the protein and mRNA levels of TRAP, cathepsin K, MMP-2, and MMP-9 were decreased in the miR-21-5p overexpression group and increased in the anti-miR-21-5p group compared with those in control cells (Fig. 2, D and E) (19).

The migration rate of osteoclast precursors was positively correlated with the differentiation and activity of osteoclasts, while the Transwell assays showed that the migration rate of osteoclast precursors transfected with miR-21-5p was decreased and that of cells transfected with anti-miR-21-5p increased (Fig. 2F) (20). Bone slices were covered with BMM cells transfected with miR-21-5p or anti-miR-21-5p and induced by M-CSF and RANKL. Following miR-21-5p inhibition, the osteoclast activity became stronger, while deeper and larger depressions on the surface of the bone slices were observed, as visualized using scanning electron microscope imaging (Fig. 2G) (21). Collectively, these results demonstrate that miR-21-5p inhibits osteoclast differentiation and activity.

Inhibitory effect of miR-21-5p on osteoclasts was rescued by SKP2

The expression levels of 18 possible target genes predicted using the four databases (Fig. 3A) were measured when miR-21-5p was overexpressed in RAW264.7 cells. Genes with significantly decreased expression were selected (SOX5, NFIB, SKP2, and XKR6) (Fig. 3B). We designed the corresponding siRNA to transfect RAW264.7 cells, followed by osteoclast differentiation induction with RANKL. Among these, SKP2 inhibition successfully inhibited osteoclast differentiation (Fig. 3C). The predicted binding sites of SKP2 are shown in Figure 3D. Si SKP2 was transfected into RAW264.7 cells, and the expression of SKP2 was detected using RT-qPCR (Fig. 3E). During osteoclast differentiation, SKP2 was closely correlated with cell proliferation efficiency, when its expression was inhibited, cell proliferation was decreased (Fig. 3F). In addition, the expression levels of TRAP, cathepsin K, MMP2, and MMP9 also decreased following SKP2 inhibition (Fig. 3, G and H). In the Transwell experiment, when the expression of SKP2 was decreased, the migration ability of preosteoclasts also decreased (Fig. 3I). The bone absorption assay showed that SKP2 was involved in osteoclast activity, which was decreased upon SKP2 inhibition (Fig. 3J). This suggests that SKP2 affected the growth, differentiation, and function of osteoclasts.

Next, we designed a rescue experiment to determine whether miR-21-5p acts on osteoclasts by regulating SKP2. The expression of SKP2 was detected using RT-qPCR (Fig. 3K). Cell proliferation was increased when miR-21-5p and SKP2 were transfected at the same time (Fig. 3L). This

rescue effect of SKP2 was confirmed by the large number of TRAP-positive multinucleated cells in the cotransfection group (Fig. 3M). Changes in osteoclast and migration-related proteins and mRNAs corresponded to the patterns observed at the cellular level (Fig. 3, N and O). When SKP2 was overexpressed, the migration and invasion abilities of osteoclast precursors were enhanced (Fig. 3P); bone absorption assay showed that the osteoclast activity was inhibited when miR-21-5p was overexpressed; however, SKP2 reversed this effect (Fig. 3Q). This suggests that miR-21-5p can inhibit osteoclasts possibly by targeting SKP2.

MiR-21-5p suppressed the development of osteoporosis in OVX mice

We selected 40 healthy 6-week-old female mice and excised their ovaries bilaterally via a small mid-back incision (Fig. 4A) (22). After 8 weeks, OVX mice were fully recovered and randomly divided into two groups, of which one was injected with precontrol via the tail vein, and the other received pre-miR-21-5p intravenously, once a week for 8 weeks. The groups were further randomly divided into two subgroups, each of which was injected with either AD control or AD SKP2 via the tail vein, once a week for 8 weeks (Fig. 4B). After the mice were sacrificed, the humerus was collected to extract RNA, and the femurs for microCT analysis, of which the right femurs were sectioned and stained. First, we detected the expression levels of miR-21-5p and SKP2, which were consistent with the injected drugs: The expression levels of miR-21-5p and SKP2 have increased accordingly (Fig. 4, C and D). Furthermore, the microCT results showed that the increased expression of miR-21-5p inhibited osteoporosis; conversely, the increased expression of SKP2 promoted its progression. In addition, our results also demonstrated that miR-21-5p could prevent osteoporosis by targeting SKP2 (Fig. 4E). The sectioned bone tissues were stained with H&E, anti-TRAP, and anti-cathepsin K antibodies. We observed several osteoclasts scattered in the bone cavity of osteoporotic mice. Importantly, miR-21-5p and SKP2 inhibited and promoted the growth of osteoclasts, respectively; miR-21-5p inhibited osteoclastogenesis via SKP2 (Fig. 4F). In addition, RT-qPCR and western blot results showed that miR-21-5p inhibited the expression of TRAP and cathepsin K, while SKP2 promoted their expression. This effect was mediated by the regulatory effect of miR-21-5p on SKP2 (Fig. 4, G–I). Overall, our *in vivo* results further show that miR-21-5p and SKP2 negatively and positively impact osteoclasts, respectively, and that SKP2 is a downstream target of miR-21-5p.

Discussion

After screening for miRNAs differentially expressed during osteoclast differentiation using gene chip technology, we found that the level of miR-21-5p was significantly decreased in mature osteoclasts, suggesting a potential role in osteoclastogenesis. This role was confirmed by *in vitro* experiments in which miR-21-5p overexpression significantly inhibited the differentiation and activity of osteoclasts at the molecular level.

Moreover, one of the predicted target genes of miR-21-5p, *SKP2*, was significantly upregulated during osteoclast differentiation, and its overexpression reversed the inhibitory effect of miR-21-5p. Collectively, these results indicate that miR-21-5p may act on osteoclast differentiation through *SKP2*, highlighting it as a potential therapeutic target for osteoporosis. The degree of osteoporosis in the femur bone was reduced in an OVX mouse model injected with pre-miR-21-5p, demonstrating the effects of miRNA on osteoporosis.

More than 2000 mature miRNAs have been identified in the human body to date, which regulate more than 50% of all protein-coding genes. Accumulating evidence has demonstrated that miRNAs regulate osteoclast differentiation, maturation, and apoptosis through complex signaling pathway networks (23). For example, miR-214-3p transferred from osteoclasts inhibited the activity of osteoblasts *in vitro* and reduced bone formation *in vivo* (24); TGFβ1/SMAD4 signaling has been shown to affect osteoclast differentiation by regulating the expression of miR-155 (25). In addition, miR-506 regulates osteoclast formation by targeting SIRT1 expression and modulating the TRPV1 channel, reactive oxygen species production, and TNF-α (26). Although the influence of miRNAs on osteoclasts has been extensively studied, data on targeted regulation of miRNAs in osteoclasts for osteoporosis treatment remain limited.

In cancer, *SKP2* acts as a proto-oncogene. When the expression of *SKP2* is decreased, the invasion and lung metastasis of osteosarcoma are inhibited (27). *SKP2* is a potential therapeutic target to inhibit the invasion of cancer cells and enhance drug sensitivity. However, data on its role in osteoclast differentiation are limited. Target genes related to miR-21-5p can be influenced through microRNAs to treat osteoporosis. Selective inhibition of *SKP2* expression can inhibit the differentiation of osteoclasts.

Although our study suggests miR-21-5p as a promising therapeutic targeted against osteoporosis, the development of miRNA-based drugs remains challenging. Importantly, miRNAs do not follow a "one-to-one" model of targets but rather a "one-to-many" model; hence, a given miRNA will induce side effects on other target genes. No methods are currently available for controlling this side effect, and the severity of potential effects remains unknown (28), which warrant further investigations.

Experimental procedures

Cell culture

The mouse macrophage cell line RAW264.7 was obtained from the Cell Bank of the Chinese Academy of Sciences (CBTCCCAS). RAW264.7 cells were cultured in minimum essential medium-alpha modified (α-MEM) containing 10% fetal bovine serum (FBS). RAW264.7 cells were treated with 50 ng/ml RANKL (R&D Systems) to induce their differentiation into osteoclasts.

Tartrate-resistant acid phosphatase (TRAP) staining assay

On the fifth day of differentiation, the osteoclasts were fixed in 4% paraformaldehyde for 20 min at room temperature (25 °C) and then stained for TRAP (Sigma) and incubated at 37 °C for 1 h. After staining, the TRAP solution was discarded, and the cells were washed with phosphate-buffered saline (Sigma) three times. TRAP-positive multinucleated cells were then observed and counted under an inverted microscope.

Transient transfection

The miR-21-5p mimetic, anti-miR-21-5p, and *SKP2* mRNA vectors were synthesized by RIBO Biotech. iMAXTransfection Reagent was used to transfect the cells for 24 h according to the manufacturer's instructions.

Cell viability assay

About 1000 cells were seeded and cultured in 96-well plates for 0, 24, 72, and 120 h to measure the growth rate after transfection. Cell viability was assessed with the Cell Counting Kit-8 (CCK-8) assay (Dojindo Molecular Technology); 10% CCK-8 reagent was added to each well and the cells were incubated at 37 °C for an additional 2 h. The optical density value of cells was directly detected on an ELx800 Absorbance Microplate Reader (BioTek Instruments) at 450 nm.

Transwell invasion assay

The migration rate of osteoclast precursors is also an important index for evaluating the activity of osteoclasts. A 200-μL cell suspension without FBS (10,000 cells/ml) was added to the inner chamber of the Transwell plate, and the lower chamber was filled with empty medium containing 10% FBS. After 24 h of incubation, the lower surface of the chamber membrane was fixed with 4% paraformaldehyde and stained with 0.1% crystal violet, and invading cells were observed under a bright-field microscope.

Bone absorption assay

BMM cells (10,000 cells/cm^2) were covered on the surface of the bone slices and then induced to differentiate by M-CSF (100 ng/ml) and RANKL (50 ng/ml) after transfection. After cell culture, adherent cells were cleaned with trypsin and sonication. The depression on the surface of the bone slice was scanned using an electron microscope (HITACHI, TM-1000), and the images obtained were quantitatively analyzed with ImageJ (NIH).

Reverse transcription–quantitative polymerase chain reaction (RT-qPCR)

RNA was extracted from the cells in each group, and 1 μg total RNA was reverse-transcribed into cDNA using 2 μl of 5X PrimeScript RT Master Mix (Takara Bio) and 4 μl RNase-free distilled water to obtain a total volume of 10 μl. The cDNA was then used as a template in qPCR on an ABI Prism 7500 system (Applied Biosystems) with SYBR Green QPCR Master Mix (Takara Bio). Glyceraldehyde 3-phosphate dehydrogenase (*Gapdh*) was used as a normalization control gene.

The primer sequences were as follows: *SKP2* (forward: 5'-TTGTTCTCCCAGTCACCCTCC-3' and reverse: 5'-AGCC
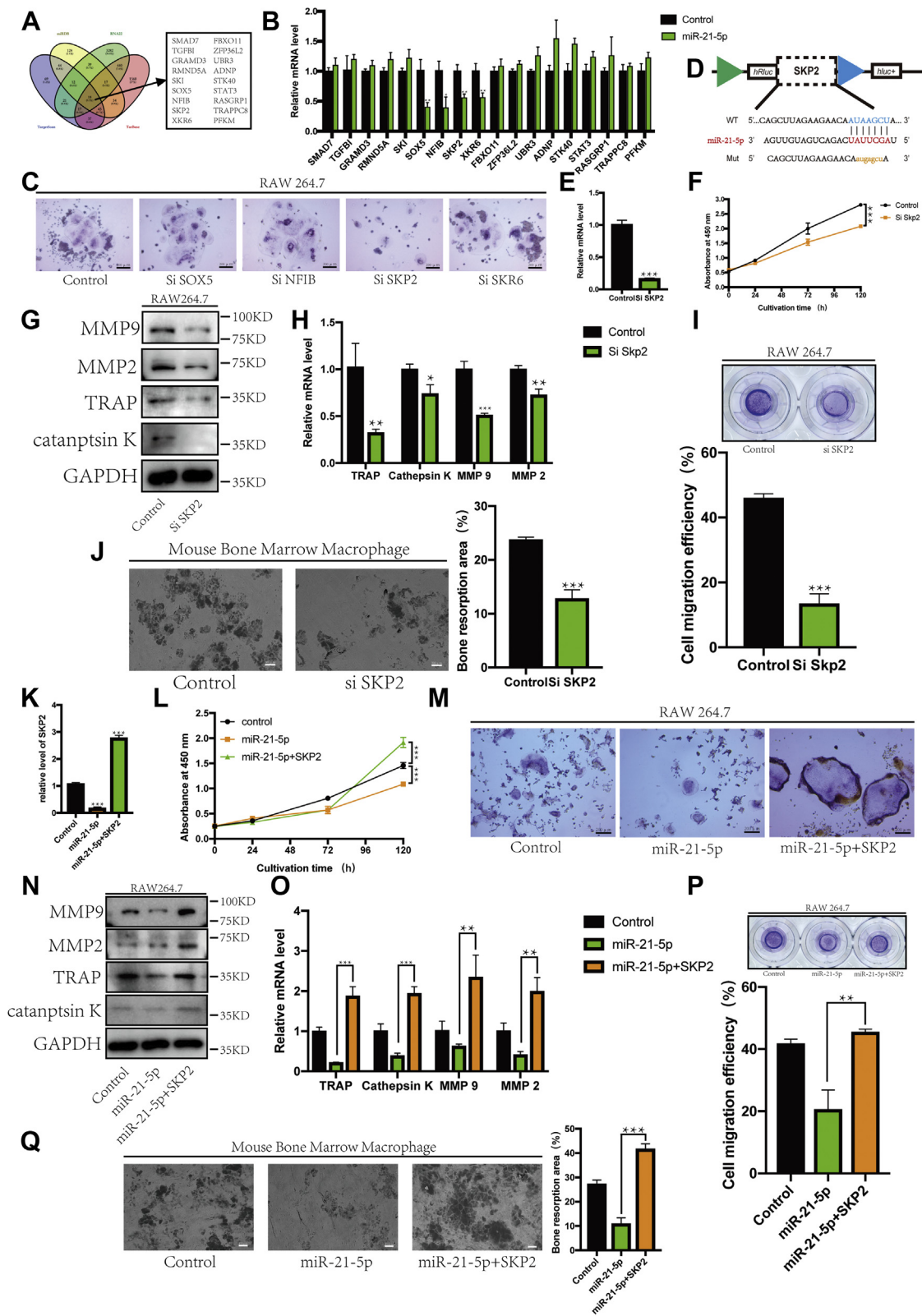
Figure 3. Inhibitory effect of miR-21-5p on osteoclasts was rescued by *SKP2*. *A*, target genes of miR-21-5p predicted by four online analysis tools. *B*, when miR-21-5p was overexpressed, the expression of selected target genes was detected by RT-qPCR. *C*, representative images of TRAP-positive multinucleated cells after transfection with corresponding siRNA (scale bar, 200 μm). *D*, target gene binding sites were predicted based on TargetScan. *E*, Si SKP2 was transfected into RAW264.7 cells, and the expression of SKP2 was detected using RT-qPCR. *F*, the CCK-8 assay was used to detect the proliferation of RAW264.7 cells. The protein and gene expression levels of TRAP, cathepsin K, MMP-9, and MMP-2 were determined by (*G*) western blot and (*H*) RT-qPCR. *Gapdh* was used as an internal reference gene. Migration was detected by (*I*) a Transwell assay, and migration efficiency was analyzed quantitatively. *J*, bone resorption test showed different pit sizes, which represented the activity of osteoclasts (scale bar, 500 μm). The defect area was analyzed quantitatively. *K*, RT-qPCR was used to determine the relative *SKP2* mRNA levels. *L*, the CCK-8 assay was used to detect the proliferation of
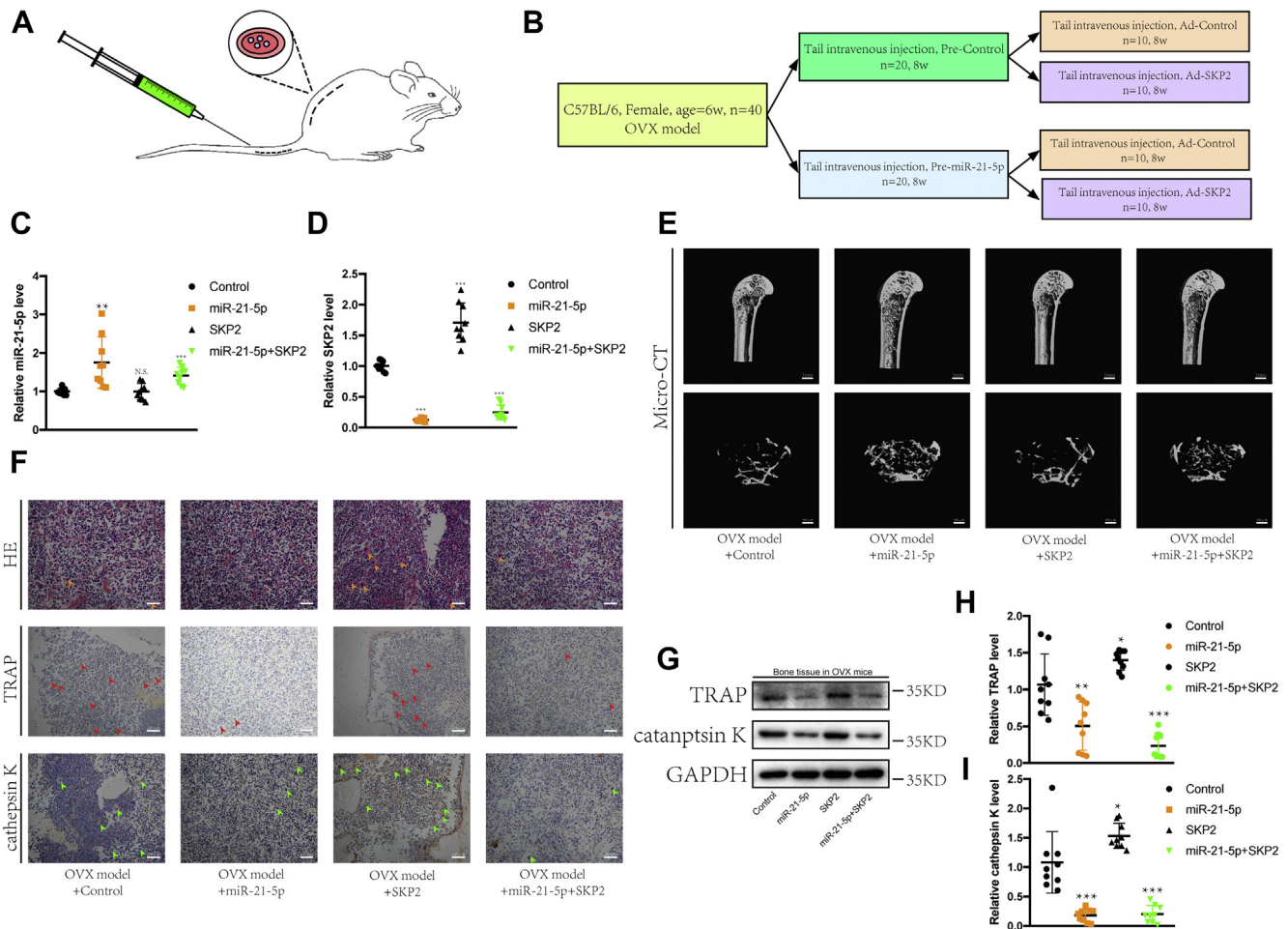
Figure 4. MiR-21-5p reversed the development of osteoporosis in OVX mice. *A*, diagram of the animal operation procedures (OVX model, tail vein injection). *B*, experiment grouping and flow chart of tail vein drug injections. RT-qPCR was used to detect the expression of miR-21-5p (*C*) and *SKP2* (*D*). *E*, microCT showed osteoporosis in mice femurs (scale bar, 1 mm, 100 μm). *F*, H&E staining, anti-TRAP staining, and anti-cathepsin K staining of fixed and decalcification femur sections (scale bar, 200 μm). *Arrows* point to osteoclasts. *G–I*, RT-qPCR and western blot were used to detect the expression of TRAP and cathepsin K. (*$p < 0.05$, **$p < 0.01$, ***$p < 0.001$. Data represent mean ± S.D. and the *p* values were determined using a two-tailed unpaired Student's *t*-test.)

GTGGACTAAAGATAGGCA-3′), *Trap* (forward: 5′- GACC-CACCGCCAAGATGGAT-3′ and reverse: 5′- CACGGTTCT GGCGATCTCTT-3′), cathepsin K (forward: 5′- TCCGCAA TCCTTACCGAATA-3′ and reverse: 5′-AACTTGAACAC CCACATCCTG-3′), matrix metalloproteinase (*Mmp*)9 (forward: 5′- CGCTCATGTACCCGCTGTAT-3′ and reverse: 5′- C CGTGGGAGGTATAGTGGGA-3′), *Mmp2* (forward: 5′-CCA CGGGCCCTATCATCTTC-3′ and reverse: 5′- CAGCACCT TTCTTTGGGCAC-3′), *Gapdh* (forward: 5′- AGCAAGGA-CACTGAGCAAGA-3′ and reverse: 5′- GGGGTCTGGGATG-GAAATTGT-3′), *miR-21-5p* (forward: 5′-CCGCGTAGC TTATCAGACTGATGTTGA-3′).

Western blot analysis

Total protein was extracted from the cells by mixing with radioimmunoprecipitation assay lysis buffer (Sigma-Aldrich),

and the supernatant was collected after centrifugation at 12,000*g* for 15 min. The proteins were separated using 10% sodium dodecyl sulfate–polyacrylamide gel electrophoresis and transferred onto a polyvinylidene fluoride membrane (Bio-Rad). The membrane was blocked with 5% skim milk powder in TBST (50 mm Tris, pH 7.6; 150 mM NaCl; 0.1% Tween 20) at room temperature for 1 h and incubated with the primary antibodies against osteoclast-related proteins TRAP, cathepsin K, MMP-2, and MMP-9 at 4 °C overnight (1:1,000, Abcam). Cathepsin K and TRAP are important indicators of osteoclast activity, and MMP-2 and MMP-9 reflect cell migration ability. After washing with TBST, the membrane was further incubated with the secondary antibody at room temperature for 2 h. The protein bands were visualized with an LAS-4000 Science Imaging System (Fujifilm) and analyzed with ImageJ software (National Institutes of Health).

RAW264.7 cells. *M*, representative images of TRAP-positive multinucleated cells are shown (scale bar, 200 μm). The protein and gene expression levels of TRAP, cathepsin K, MMP-9, and MMP-2 were determined by (*N*) western blot and (*O*) RT-qPCR. *Gapdh* was used as an internal reference gene. Migration was detected by (*P*) a Transwell assay, and migration efficiency was analyzed quantitatively. *Q*, bone resorption test showed different pit sizes, which represented the activity of osteoclasts (scale bar, 500 μm). The defect area was analyzed quantitatively. (*$p < 0.05$, **$p < 0.01$, ***$p < 0.001$. Data represent mean ± S.D. and the *p* values were determined using a two-tailed unpaired Student's *t*-test.)

MiR-21-5p inhibits osteoclastogenesis via SKP2

Target prediction

To explore the mechanisms by which miR-21-5p affects osteoclast differentiation, we used three separate databases to identify miR-21-5p target genes: TargetScan (http://www.targetscan.org), miRTarBase (http://mirtarbase.mbc.nctu.edu.tw/php/index.php), RNA22 (https://cm.jefferson.edu/rna22/Interactive/), and miRDB (http://www.mirdb.org/) (29).

Animal model

We established an OVX-induced osteoporosis model to determine the effects of miR-21-5p on osteoporosis *in vivo*. All animal experiments were performed in accordance with the principles and procedures of the National Institutes of Health Guide for the Care and Use of Laboratory Animals and the guidelines for the animal treatment of Sir Run Shaw Hospital (Zhejiang University affiliated, Hangzhou, Zhejiang). The bilateral ovaries were removed through an incision on the back of 8-week-old female C57 mice to establish an OVX model.

In brief, the mice were anesthetized by intraperitoneal injection of 10% chloral hydrate (0.4 ml/100 g) and placed in the prone position. The hair was cut at 0.5 cm above the inner side of the thigh root on the back, the skin was sterilized and cut, and the muscle was separated bluntly. The ovary was stripped and removed after the uterus was ligated to stop the bleeding. The muscle layer and skin incision were sutured, and penicillin was injected to prevent infection. The other ovary was removed following the same procedure.

The adenovirus precontrol, pre-miR-21-5p, control, and *SKP2* were constructed and provided by Hanbio Biotechnology (Shanghai) Co, Ltd. After successful OVX modeling, mice were intraperitoneally injected with adenovirus solution once a week for 8 weeks. A 100 μl solution containing circSPG21-wt or -mut was slowly injected into the abdominal cavity.

Statistical analysis

Data represent mean ± standard deviation (SD) and the p values were determined with a two-tailed unpaired Student's t-test (using the 95% confidence interval of the difference between groups) using SPSS v22.0. Differences between groups with $p < 0.05$ were considered statistically different.

Data availability

All data included in this study are available upon request by contact with the corresponding author.

Author contributions—J. M. and S. S. conceived and supervised the study; Y. H. designed the experiments; Y. H., Y. Y., and T. Y. performed the experiments; Y. X. provided new tools and reagents; J. G. developed new software and performed simulation studies; Y. H. analyzed the data; S. Y. and P. Y. wrote the article; J. M. and S. S. revised the article.

Abbreviations—The abbreviations used are: α-MEM, minimum essential medium-alpha modified; CCK-8, cell counting kit-8; CTSK, cathepsin K; FBS, fetal bovine serum; GAPDH, glyceraldehyde 3-phosphate dehydrogenase; HE, haematoxylin and eosin; miRNAs, microRNAs; MMP, matrix metalloproteinase; OVX, ovariectomized; RANKL, receptor activator of nuclear factor kappa B ligand; RT-qPCR, reverse transcription–quantitative polymerase chain reaction; siRNAs, small interfering RNAs; TRAP, tartrate-resistant acid phosphatase.

References

1. Datta, H. K., Ng, W. F., Walker, J. A., Tuck, S. P., and Varanasi, S. S. (2008) The cell biology of bone metabolism. *J. Clin. Pathol.* **61**, 577–587
2. Armas, L. A., and Recker, R. R. (2012) Pathophysiology of osteoporosis: New mechanistic insights. *Endocrinol. Metab. Clin. North Am.* **41**, 475–486
3. Li, L., and Wang, Z. (2018) Ovarian aging and osteoporosis. *Adv. Exp. Med. Biol.* **1086**, 199–215
4. Weaver, C. M., Alexander, D. D., Boushey, C. J., Dawson-Hughes, B., Lappe, J. M., LeBoff, M. S., Liu, S., Looker, A. C., Wallace, T. C., and Wang, D. D. (2016) Calcium plus vitamin D supplementation and risk of fractures: An updated meta-analysis from the National Osteoporosis Foundation. *Osteoporos. Int.* **27**, 367–376
5. Muñoz-Torres, M., Alonso, G., and Raya, M. P. (2004) Calcitonin therapy in osteoporosis. *Treat. Endocrinol.* **3**, 117–132
6. Yuan, F., Peng, W., Yang, C., and Zheng, J. (2019) Teriparatide versus bisphosphonates for treatment of postmenopausal osteoporosis: A meta-analysis. *Int. J. Surg.* **66**, 1–11
7. Väänänen, H. K., and Härkönen, P. L. (1996) Estrogen and bone metabolism. *Maturitas* **23 Suppl**, S65–S69
8. Mohr, A. M., and Mott, J. L. (2015) Overview of microRNA biology. *Semin. Liver Dis.* **35**, 3–11
9. Lian, W. S., Ko, J. Y., Chen, Y. S., Ke, H. J., Hsieh, C. K., Kuo, C. W., Wang, S. Y., Huang, B. W., Tseng, J. G., and Wang, F. S. (2019) MicroRNA-29a represses osteoclast formation and protects against osteoporosis by regulating PCAF-mediated RANKL and CXCL12. *Cell Death Dis.* **10**, 705
10. Xiao, Y., Li, B., and Liu, J. (2018) MicroRNA-148a inhibition protects against ovariectomy-induced osteoporosis through PI3K/AKT signaling by estrogen receptor α. *Mol. Med. Rep.* **17**, 7789–7796
11. Li, J. Y., Wei, X., Sun, Q., Zhao, X. Q., Zheng, C. Y., Bai, C. X., Du, J., Zhang, Z., Zhu, L. G., and Jia, Y. S. (2019) MicroRNA-449b-5p promotes the progression of osteoporosis by inhibiting osteogenic differentiation of BMSCs via targeting Satb2. *Eur. Rev. Med. Pharmacol. Sci.* **23**, 6394–6403
12. Cai, Z., Moten, A., Peng, D., Hsu, C. C., Pan, B. S., Manne, R., Li, H. Y., and Lin, H. K. (2020) The Skp2 pathway: A critical target for cancer therapy. *Semin. Cancer Biol.* **67**, 16–33
13. Li, C., Du, L., Ren, Y., Liu, X., Jiao, Q., Cui, D., Wen, M., Wang, C., Wei, G., Wang, Y., Ji, A., and Wang, Q. (2019) SKP2 promotes breast cancer tumorigenesis and radiation tolerance through PDCD4 ubiquitination. *J. Exp. Clin. Cancer Res.* **38**, 76
14. Thacker, G., Kumar, Y., Khan, M. P., Shukla, N., Kapoor, I., Kanaujiya, J. K., Lochab, S., Ahmed, S., Sanyal, S., Chattopadhyay, N., and Trivedi, A. K. (2016) Skp2 inhibits osteogenesis by promoting ubiquitin-proteasome degradation of Runx2. *Biochim. Biophys. Acta* **1863**, 510–519

15. Yin, Z., Zhu, W., Wu, Q., Zhang, Q., Guo, S., Liu, T., Li, S., Chen, X., Peng, D., and Ouyang, Z. (2019) Glycyrrhizic acid suppresses osteoclast differentiation and postmenopausal osteoporosis by modulating the NF-κB, ERK, and JNK signaling pathways. *Eur. J. Pharmacol.* **859**, 172550

16. Chen, X., Ouyang, Z., Shen, Y., Liu, B., Zhang, Q., Wan, L., Yin, Z., Zhu, W., Li, S., and Peng, D. (2019) CircRNA_28313/miR-195a/CSF1 axis modulates osteoclast differentiation to affect OVX-induced bone absorption in mice. *RNA Biol.* **16**, 1249–1262

17. Wang, L., Gao, Z., Zhang, J., Huo, Y., Xu, Q., and Qiu, Y. (2021) Netrin-1 regulates ERK1/2 signaling pathway and autophagy activation in wear particle-induced osteoclastogenesis. *Cell Biol. Int.* **45**, 612–622

18. Song, C., Yang, X., Lei, Y., Zhang, Z., Smith, W., Yan, J., and Kong, L. (2019) Evaluation of efficacy on RANKL induced osteoclast from RAW264.7 cells. *J. Cell Physiol.* **234**, 11969–11975

19. Sun, L., Lian, J. X., and Meng, S. (2019) MiR-125a-5p promotes osteoclastogenesis by targeting TNFRSF1B. *Cell. Mol. Biol. Lett.* **24**, 23

20. Gan, K., Yang, L., Xu, L., Feng, X., Zhang, Q., Wang, F., Tan, W., and Zhang, M. (2016) Iguratimod (T-614) suppresses RANKL-induced osteoclast differentiation and migration in RAW264.7 cells via NF-κB and MAPK pathways. *Int. Immunopharmacol.* **35**, 294–300

21. Xie, Z., Yu, H., Sun, X., Tang, P., Jie, Z., Chen, S., Wang, J., Qin, A., and Fan, S. (2018) A novel diterpenoid suppresses osteoclastogenesis and promotes osteogenesis by inhibiting Ifrd1-mediated and IκBα-mediated p65 nuclear translocation. *J. Bone Miner. Res.* **33**, 667–678

22. Li, J., Li, X., Liu, D., Hamamura, K., Wan, Q., Na, S., Yokota, H., and Zhang, P. (2019) eIF2α signaling regulates autophagy of osteoblasts and the development of osteoclasts in OVX mice. *Cell Death Dis.* **10**, 921

23. Kabekkodu, S. P., Shukla, V., Varghese, V. K., D' Souza, J., Chakrabarty, S., and Satyamoorthy, K. (2018) Clustered miRNAs and their role in biological functions and diseases. *Biol. Rev. Camb. Philos. Soc.* **93**, 1955–1986

24. Li, D., Liu, J., Guo, B., Liang, C., Dang, L., Lu, C., He, X., Cheung, H. Y., Xu, L., Lu, C., He, B., Liu, B., Shaikh, A. B., Li, F., Wang, L., *et al.* (2016) Osteoclast-derived exosomal miR-214-3p inhibits osteoblastic bone formation. *Nat. Commun.* **7**, 10872

25. Zhao, H., Zhang, J., Shao, H., Liu, J., Jin, M., Chen, J., and Huang, Y. (2017) Transforming growth factor β1/Smad4 signaling affects osteoclast differentiation via regulation of miR-155 expression. *Mol. Cells* **40**, 211–221

26. Yan, S., Miao, L., Lu, Y., and Wang, L. (2019) MicroRNA-506 upregulation contributes to sirtuin 1 inhibition of osteoclastogenesis in bone marrow stromal cells induced by TNF-α treatment. *Cell Biochem. Funct.* **37**, 598–607

27. Zhang, Y., Zvi, Y. S., Batko, B., Zaphiros, N., O'Donnell, E. F., Wang, J., Sato, K., Yang, R., Geller, D. S., Koirala, P., Zhang, W., Du, X., Piperdi, S., Liu, Y., Zheng, D., *et al.* (2018) Down-regulation of Skp2 expression inhibits invasion and lung metastasis in osteosarcoma. *Sci. Rep.* **8**, 14294

28. Zhang, Y., Wang, Z., and Gemeinhart, R. A. (2013) Progress in microRNA delivery. *J. Control. Release* **172**, 962–974

29. Wang, S., Shen, L., and Luo, H. (2021) Identification and validation of key miRNAs and a microRNA-mRNA regulatory network associated with ulcerative colitis. *DNA Cell Biol.* **40**, 147–156